Displacement Damage Effects in Solar Cells—Mining Damage From the Microelectronics and Photonics Test Bed Space Experiment

R.J. Walters
Naval Research Laboratory, Washington, DC

T.L. Morton
Ohio Aerospace Institute, Cleveland, OH

S.R. Messenger
SFA, Inc., Largo, MD

The NASA STI Program Office…in Profile

Since its founding, NASA has been dedicated to the advancement of aeronautics and space science. The NASA Scientific and Technical Information (STI) Program Office plays a key part in helping NASA maintain this important role.

The NASA STI Program Office is operated by Langley Research Center, the lead center for NASA's scientific and technical information. The NASA STI Program Office provides access to the NASA STI Database, the largest collection of aeronautical and space science STI in the world. The Program Office is also NASA's institutional mechanism for disseminating the results of its research and development activities. These results are published by NASA in the NASA STI Report Series, which includes the following report types:

- TECHNICAL PUBLICATION. Reports of completed research or a major significant phase of research that present the results of NASA programs and include extensive data or theoretical analysis. Includes compilations of significant scientific and technical data and information deemed to be of continuing reference value. NASA's counterpart of peer-reviewed formal professional papers but has less stringent limitations on manuscript length and extent of graphic presentations.

- TECHNICAL MEMORANDUM. Scientific and technical findings that are preliminary or of specialized interest, e.g., quick release reports, working papers, and bibliographies that contain minimal annotation. Does not contain extensive analysis.

- CONTRACTOR REPORT. Scientific and technical findings by NASA-sponsored contractors and grantees.

- CONFERENCE PUBLICATION. Collected papers from scientific and technical conferences, symposia, seminars, or other meetings sponsored or cosponsored by NASA.

- SPECIAL PUBLICATION. Scientific, technical, or historical information from NASA programs, projects, and mission, often concerned with subjects having substantial public interest.

- TECHNICAL TRANSLATION. English-language translations of foreign scientific and technical material pertinent to NASA's mission.

Specialized services that complement the STI Program Office's diverse offerings include creating custom thesauri, building customized databases, organizing and publishing research results…even providing videos.

For more information about the NASA STI Program Office, see the following:

- Access the NASA STI Program Home Page at *http://www.sti.nasa.gov*

- E-mail your question via the Internet to help@sti.nasa.gov

- Fax your question to the NASA Access Help Desk at 301–621–0134

- Telephone the NASA Access Help Desk at 301–621–0390

- Write to:
  NASA Access Help Desk
  NASA Center for AeroSpace Information
  7121 Standard Drive
  Hanover, MD 21076–1320
  301–621–0390

Displacement Damage Effects in Solar Cells—Mining Damage From the Microelectronics and Photonics Test Bed Space Experiment

R.J. Walters
Naval Research Laboratory, Washington, DC

T.L. Morton
Ohio Aerospace Institute, Cleveland, OH

S.R. Messenger
SFA, Inc., Largo, MD

Acknowledgments

TRADEMARKS

Available from:

NASA Center for AeroSpace Information	National Technical Information Service
7121 Standard Drive	5285 Port Royal Road
Hanover, MD 21076–1320	Springfield, VA 22161
(301) 621–0390	(703) 487–4650

TABLE OF CONTENTS

LIST OF FIGURES

LIST OF TABLES

LIST OF ACRONYMS AND SYMBOLS

a-Si   amorphous silicon

CIGS $CuIn(Ga)Se_2$

CREDO   Cosmic Radiation Environment and Dosimetry

CRRES   Combined Release and Radiation Effects Satellite

DSU   data service unit

EOL   end of life

GaAs   gallium arsenide

Ge   germanium

GRC   Glenn Research Laboratory

GUI   graphical user interface

I-load   current load

InGaP   indium gallium phosphide

IPE   Institute of Photovoltaic Energy

JPL   Jet Propulsion Laboratory

MPTB   Microelectronics and Photonics Test Bed

MJ   multijunction

NIEL   nonionizing energy loss

NRL   Naval Research Laboratory

OAI   Ohio Aerospace Institute

PV   photovoltaic

RDC   relative damage coefficient

SAVANT   Solar Array Verification and Analysis Tool

Si   silicon

SJ	single junction
SPL	Spectrolab
SRIM	stopping and range of ions in matter
TFSC	thin film solar cells

NOMENCLATURE

C	fitting parameter
dC	uncertainty calculation of C
Dd	damage displacement dose
$dDxe$	uncertainty calculation of Dxe
$dDxp$	uncertainty calculation of Dxp
Dx	fitting parameter
Dxe	electron Dx
Dxp	proton Dx
Imp	current at maximum power
Isc	short circuit current
Isc_0	solar cell short circuit current prior to irradiation
M	mean anomaly
n	parameter
P_0	initial value of photovoltaic parameter in question
P_{max}	maximum power
Pmp	maximum power point
r	Sun-Earth separation as a function of time
Rep	factor used to convert an electron Dd value to an equivalent proton Dd value
T	period
t	time
Vmp	voltage at maximum power
Voc	open circuit voltage
ε	eccentricity of Earth's orbit
ζ	parameter
ζ_0	parameter
η	parameter
ψ	eccentric anomaly

TECHNICAL PUBLICATION

DISPLACEMENT DAMAGE EFFECTS IN SOLAR CELLS—MINING DAMAGE FROM THE MICROELECTRONICS AND PHOTONICS TEST BED SPACE EXPERIMENT

1. INTRODUCTION

The United States Naval Research Laboratory (NRL), in collaboration with the Ohio Aerospace Institute (OAI) and NASA Glenn Research Center (GRC), has executed a 1-yr program to develop an improved space solar cell radiation response analysis capability and to produce a computer modeling tool which implements the analysis. This was accomplished, in part, through analysis (mining) of solar cell flight data taken on the Microelectronics and Photonics Test Bed (MPTB) experiment. This project is funded by the NASA Living with a Star Space Environment Test Bed, NRA8–3, and is responsive to the goal "to infuse the predictive capability and technology validation results in space…to government and industry users…for spacecraft design and operations." This project specifically addresses issues related to rapid technological change in the area of solar cells for space applications in order to enhance system performance, decrease risk, and reduce cost for future missions.

In this project, data of the photogenerated current from the MPTB solar array that has been telemetered to the ground from the spacecraft were analyzed. The concept of displacement damage dose (Dd) has been used, employing the methodology developed at NRL, to characterize the radiation-induced degradation to the solar array output; the computer code Solar Array Verification and Analysis Tool (SAVANT), being developed by OAI under contract to GRC, has been used to predict the solar array output. The ultimate goal of this work was to validate the SAVANT code against the measured space data and develop SAVANT into a user-friendly executable program that can be widely distributed. This Technical Publication provides the final report for this project.

2. MICROELECTRONICS AND PHOTONICS TEST BED SOLAR ARRAY DATA

The solar array onorbit under study in this project is a specific solar array mounted on the MPTB host spacecraft that is dedicated to providing power to the MPTB experiment. The array operates at a fixed voltage of 31.2 V, but the current is not controlled. Therefore, any changes in the photocurrent of the array can be detected and analyzed. The array consists of 27 strings of cells with 54 cells in each string. The 27 strings are grouped into 19 circuits with 1 to 3 strings in each circuit, depending on the fuse size used for that specific circuit. The solar cell technology is Spectrolab (SPL) 8-mil single-junction (SJ) gallium arsenide (GaAs)/germanium (Ge).

A major task of this project was to gather the massive amount of solar array data into a usable format. The data have been summarized in a Microsoft® Excel spreadsheet. The data consist of the minimum, maximum, average, and standard deviation of the solar panel voltage, current, and backside temperature. To minimize earth albedo effects, the data are restricted to those data taken near apogee.

The telemetered data shows the backside solar array temperature to vary from about 32 to 49 °C. Since the ground test data for the SPL solar cells, like the vast majority of solar cell ground test data, were taken at room temperature (28 °C) and since the photovoltaic output of a solar cell is temperature dependent, the orbital data must be corrected for temperature. Information from spacecraft engineers indicates that there is about an 11.1 °C temperature increase from the rear to the front face of the array. Therefore, the solar cell temperature was estimated to be equal to the telemetered temperature data increased by this amount. The telemetered array current data are corrected from these temperatures to room temperature using temperature coefficients, which are determined from ground test data by measuring the solar cell output at various temperatures. M.R. Brown et al.[1] published such data measured on cells nominally identical to the MPTB cells that indicated a change of about 17 $\mu A/cm^2/°C$. Communication from SPL suggested a value of 20 $\mu A/cm^2/°C$, which compares quite well. Using the published temperature coefficient data from reference 1, the on-orbit current data were corrected to 28 °C. The resultant data are plotted as a function of date in figure 1.

The next correction to make to the telemetered data is to compensate for the variation in solar intensity that occurs due to seasonal variations. This is essentially a problem of geometry. The spacecraft is assumed to be collocated with the Earth, which is an acceptable approximation given the comparison of the orbital altitude with the Sun-Earth separation distance. Then, the problem is reduced to determining the Sun-Earth separation at the time each data point was measured. The average position is 1 au and varies between $1-\varepsilon$ and $1+\varepsilon$ where ε, the eccentricity of Earth's orbit, is 0.0168.

The separation distance is calculated using Kepler's equations. Kepler's equations relate the mean anomaly, M, to the eccentric anomaly, ψ. The mean anomaly measures the angular deviation of a body moving in a circular orbit with a period T and is given by $2\pi(t/T)$. T is 1 yr, which is taken to be 365.25 days. The eccentric anomaly is used to calculate r as a function of time. The time, t, is determined as the difference in days between the measurement date and the date of Earth's perihelion. Naval Observatory
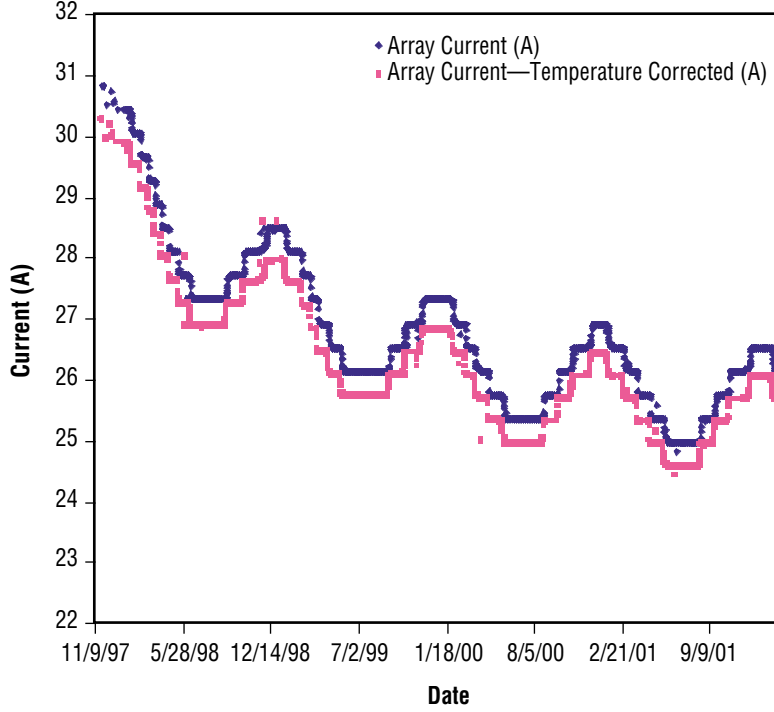
Figure 1. MPTB on-orbit solar array data before and after
temperature correction.

data give the first date of Earth's perihelion coincident with the mission time as 1/4/98. To proceed, an approximate solution of Kepler's equation must be adopted. E.W. Brown's algorithm has been chosen as described in Marion,[2] which consists of the following expressions:

$$\zeta = \zeta_0 + Arc\sin\left[\frac{\pm\varepsilon^3}{6\eta}\sin^3(M+\zeta_0)\right]$$

$$\zeta_0 = Arc\tan\left[\frac{\varepsilon\sin(M)}{1-\varepsilon\cos(M)}\right]$$

$$\eta = \sqrt{1-2\varepsilon\cos(M)+\varepsilon^2}$$

$$\psi = M + \zeta$$

$$r = 1 - \varepsilon\cos(\psi) \ , \tag{1}$$

where ε is the eccentricity of Earth's orbit and r is the Sun-Earth separation as a function of time.

To compensate for the seasonal variations, the measured data are normalized to that at the average value, using the fact that the photocurrent of the solar array varies linearly with solar intensity and that the solar intensity varies with the inverse square of distance. Therefore, the normalization consists of multiplying the measured data by the ratio of the inverse square of the average to the actual Sun-Earth distance, which, since the average distance is 1 au, reduces to multiplying the measured data by r^2. Doing this, the corrected data are thus obtained as shown in figure 2.

3
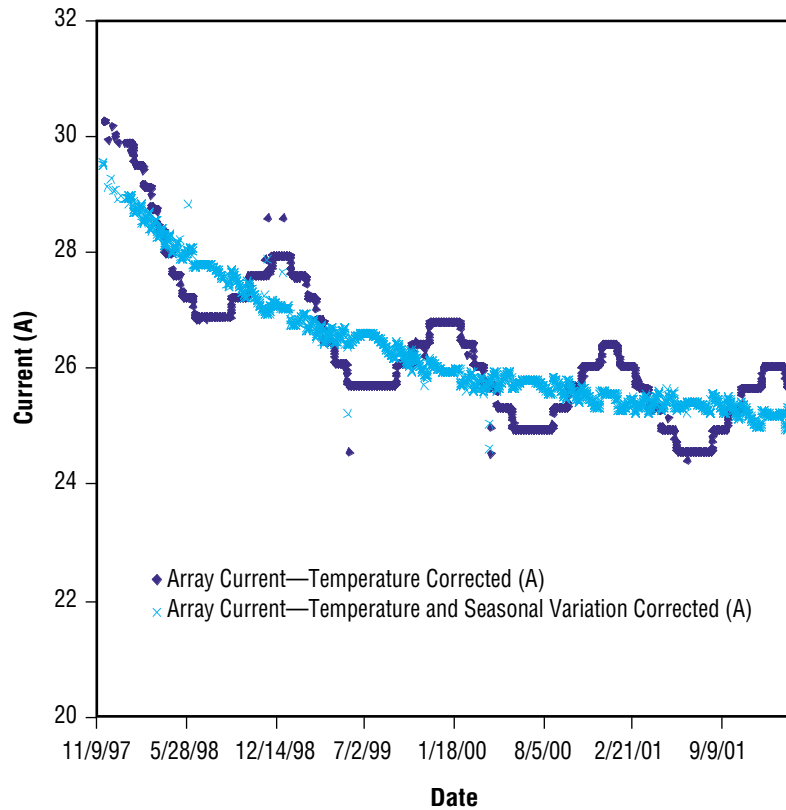
Figure 2. MPTB on-orbit solar array data after temperature
correction, before and after correction for seasonal
variations.

The correction has produced the desired effect of smoothing out the periodic oscillations. The roughly saw-toothed pattern visible in the data occurs because the original data have a distinct stairstep pattern and the plateaus at each perihelion and aphelion are long. This is due to the limited resolution of the analog to digital converter (ADC) onboard the spacecraft. The corrected data shown in figure 2 are the data which will be compared to the predictions.

4

3. GROUND TEST DATA REDUCTION AND ANALYSIS

The prediction of the performance of a solar cell in orbit is based on measurements of the solar cell output made on the ground. The ground test data reduction and analysis that were performed are described in this section. The primary purpose of the analysis is to establish the capability of predicting the response of a solar cell to irradiation by a spectrum of particles using ground test data measured after monoenergetic particle irradiation. It is this capability that constitutes the major advancement provided by the NRL method.[3]

In the NRL method, a degradation curve is generated from the monoenergetic ground test data. This curve describes the radiation response of the specific solar cell technology, and as such, is referred to as the characteristic curve. The data analysis begins with gathering the available ground test data. As a preface to presenting these data, a brief description of the parameters typically used to describe solar cells is given. Each of the parameters refers to the solar cell output at specific points along the illuminated IV curve as shown in figure 3. The current measured at short circuit is the short circuit current (*Isc*). The voltage measured at open circuit is the open circuit voltage (*Voc*). The maximum electrical power produced by the cell is referred to as the maximum power point (*Pmp*) with the associated current (*Imp*) and voltage (*Vmp*) at maximum power.

Figure 3. Typical IV curve measured on an SPL SJ GaAs solar cell with the standard photovoltaic parameters indicated on the graph.

For this effort, SPL supplied NRL with a single set of ground test data measured under 1-MeV electron irradiation. In a separate project funded by SPL, NRL measured proton irradiation data on SPL SJ GaAs/Ge solar cells. These data were measured under 0.4- and 1-MeV proton irradiation. A third dataset measured under 1-MeV electrons was taken from the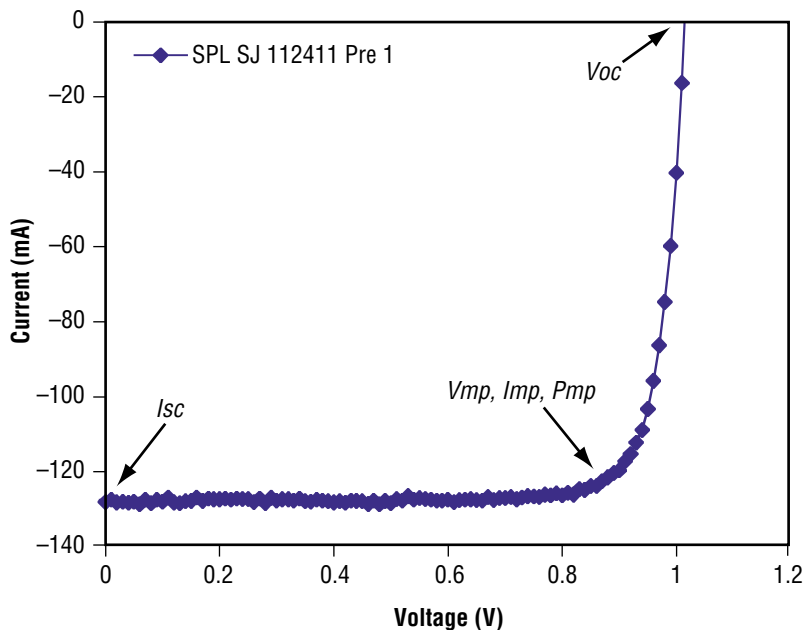 published data in reference 4. To achieve confidence in these data, consistency was established among the data by converting the proton data to an equivalent set of 1-MeV electron data. First, the proton data were converted to an equivalent 10-MeV proton fluence by multiplying the proton fluence values by the ratio of the nonionizing energy loss (NIEL) at the proton energy (either 0.4 or 1 MeV) to the NIEL at 10 MeV. This conversion is based on the damage equivalence concept within the NRL methodology. The equivalent 10-MeV proton fluence values were then converted to equivalent 1-MeV electron fluence values using the empirically determined conversion factors published in reference 4. Considering the *Isc* data, the conversion factor is 400. The resultant equivalent 1-MeV electron datasets are compared to the SPL 1-MeV electron data in figure 4 for the case of the *Isc* parameter. Up to a fluence of $\approx 1 \times 10^{15}$ cm^{-2}, all of the datasets agree very well, which supports the use of these data to characterize the MPTB solar cells.
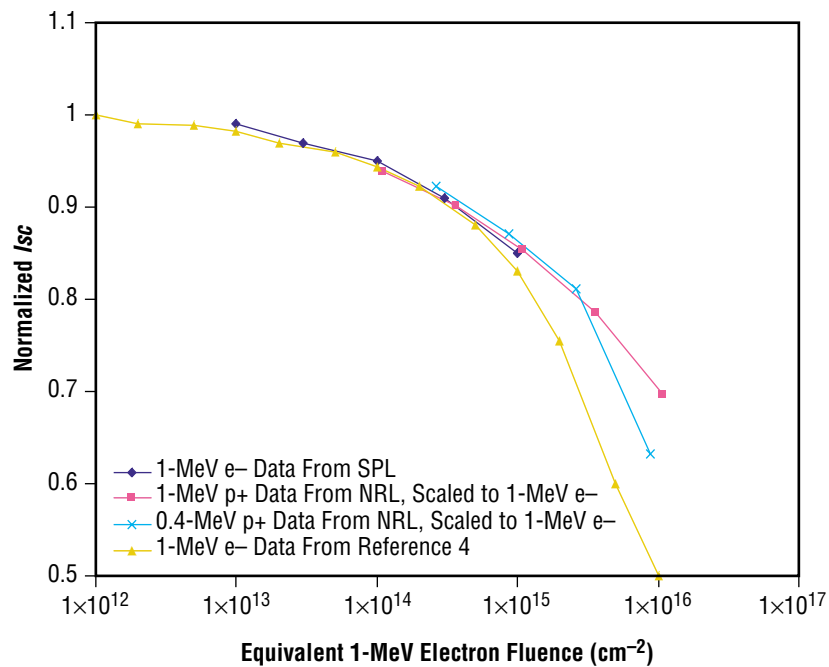
Figure 4. *Isc* data normalized to the preirradiation values from
several different irradiation datasets.

With the ground test data established, the next step in the NRL methodology is to convert the various particle fluence values to an equivalent value of *Dd*. This is accomplished by multiplying the fluence by the NIEL value for the given particle and energy. NRL has calculated the NIEL for protons and electrons incident upon GaAs.[5] For the proton data, it has been shown that a linear relationship exists between *Dd* and NIEL.[5] However, this is not necessarily the case for the electron data. As described in reference 5, the value of equivalent *Dd* for a given electron irradiation is obtained using a power law function of NIEL with the exponent referred to as the *n* parameter. For the GaAs/Ge technology used on MPTB, *n* has been calculated to be 1.7. Because of this nonlinearity between the solar cell damage coefficients and NIEL for the case of electron irradiation, the equivalent *Dd* value for a spectrum of electrons must be normalized

to a given reference energy. For solar cells, the reference electron energy is typically chosen to be 1 MeV. The *n* parameter will be required to calculate the equivalent value of *Dd* for a given electron spectrum irradiation. The radiation degradation given in figure 4 is plotted as a function of *Dd* in figure 5.
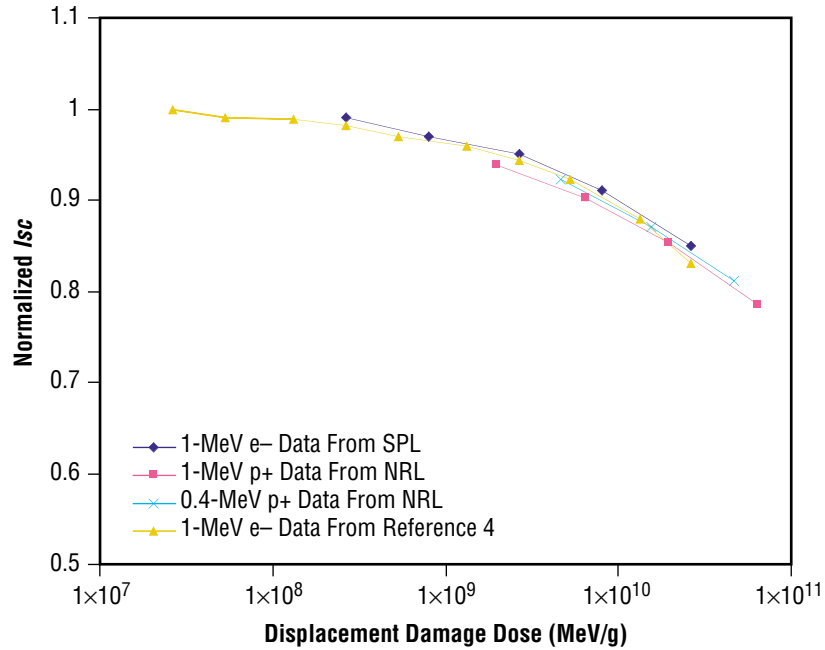
Figure 5. GaAs/Ge solar cell *Isc* data plotted as a function of *Dd*.

Figure 5 shows that the data measured after irradiation by different particles at different energies collapse to a single curve when plotted as a function of *Dd*. This curve is characteristic for this technology, and it can now be used to describe or predict the cell response in any proton or electron radiation environment; this is the foundation of the NRL method. By analyzing the data in terms of *Dd*, data from a variety of different radiations can be easily reduced to a common curve. Moreover, since the NIEL is a calculated quantity, the characteristic curve can be determined from a single proton dataset. In the case of electrons, at least two data sets are required to enable determination of the *n* parameter. From a practical standpoint, this represents an advance because it greatly reduces the amount of radiation data required to fully characterize the radiation response of a solar cell technology. Thus, the *Dd* method frees resources that can be used to generate more data points at each specific energy, which will reduce the error in the fitting procedure. It is much less expensive to perform, for example, irradiations at two energies with seven fluence points at each energy than it is to perform irradiations at eight energies with four fluences each. Therefore, the *Dd* method provides the capability to produce more accurate predictive capability at a lower cost. Also, the *Dd* analysis allows a full characterization for new technologies even though there may be very little data available.

To parameterize the characteristic curve, the data is fit to the following equation:

$$Isc / Isc_0 = 1 - C \log\left[1 + \frac{Dd}{Dx}\right],$$

(2)

7

where *C* and *Dx* are the fitting parameters and *Isc*/*Isc*$_0$ refers to the value of *Isc* measured after irradiation and normalized to the preirradiation value. This is essentially the equation presented in reference 4 except the particle fluence has been replaced by *Dd*. In the fitting procedure, the electron and proton data are typically fit separately. This is the case because, as a result of the nonlinear dependence of the electron *Dd* on NIEL, the characteristic curve for the electron data does not typically align with that from the proton data. The separation of the curves is not specifically evident in figure 5 because the separation for the *Isc* data is typically small. Larger differences are typically observed for the other photovoltaic parameters. The electron and proton data are fit such that each is described by a common value of *C* and a separate *Dx*. The proton *Dx* is designated by *Dxp* and the electron by *Dxe*. The ratio of *Dxe* to *Dxp* is referred to as the *Rep* factor, which is used to convert an electron *Dd* value to an equivalent proton *Dd* value. The fitting parameters determined for each of the GaAs photovoltaic parameters are given in table 1; the columns identified as *dC*, *dDxp*, etc., are the uncertainty associated with the calculated parameter. The *Dx* parameter is in units of MeV/g, which is the unit of *Dd*.

The data given in table 1 allow the solar cell radiation response to a given radiation environment to be analyzed in terms of the photovoltaic parameters listed. However, in a solar array, the solar cell seldom operates at short circuit, open circuit, or at the maximum power point. Instead, the array operates at a fixed bus voltage, so the cell operates at a fixed load point characterized by a load current and voltage. The data supplied from spacecraft telemetry are the solar array load current. Therefore, whether the radiation response of the solar array load current is accurately modeled by the ground test parameters must be determined. The array consists of 27 strings of 54 solar cells in each string. The SJ GaAs solar cells have a *Voc* of about 1.02 V. The array *Voc* is then 54 × 1.02 = 55.9 V. The MPTB solar array voltage is held constant at 31.2 V. Therefore, the array load point is ≈56.8 percent of *Voc*. Using this, the load voltage for an individual cell can be estimated to be 56.8 percent of *Voc* or 0.578 V. With this information, the radiation degradation of the solar cell current at this load point (I-load) may be tracked.

Table 1. Fitting parameters determined from
fitting each of the GaAs PV parameter
datasets to equation (2).

	C	*dC*	*Dxp*	*dDxp*	*Dxe*	*dDxe*	*Rep*
Isc	0.153	0.002	2.36×10^9	6×10^7	3×10^9	1×10^9	1.3
Voc	0.112	0.002	1.81×10^9	9×10^7	2×10^9	1×10^9	1.1
Imp	0.236	0.004	5.2×10^9	2×10^8	6×10^9	2×10^9	1.2
Vmp	0.128	0.002	1.9×10^9	1×10^8	3×10^9	2×10^9	1.6
Pmp	0.261	0.003	1.57×10^9	8×10^7	2.7×10^9	7×10^8	1.7

The graph in figure 6 was generated using 1-MeV proton irradiation ground test data. Each curve represents the cell output after irradiation by 1-MeV protons up to the *Dd* level given in the legend. The blue squares indicate the maximum power point, and the red diamonds indicate the load point. Note that the irradiation level associated with each IV curve is expressed in terms of *Dd* and is given in the legend. In this graph, the maximum power point and the load point on each curve have been highlighted. The two different points are seen to follow different tracks through the current-voltage space with increasing *Dd*, but since the slope of the IV curve is very small up to *Pmp*, the change in the I-load with increasing *Dd* is essentially the same as *Imp*. This is shown explicitly in figure 7 where the I-load, *Imp*, and *Isc* have been

normalized to their preirradiation value and plotted as a function of *Dd*. These data suggest that I-load tracks *Imp* closely, so the data for *Imp* will be used in the calculations that follow.
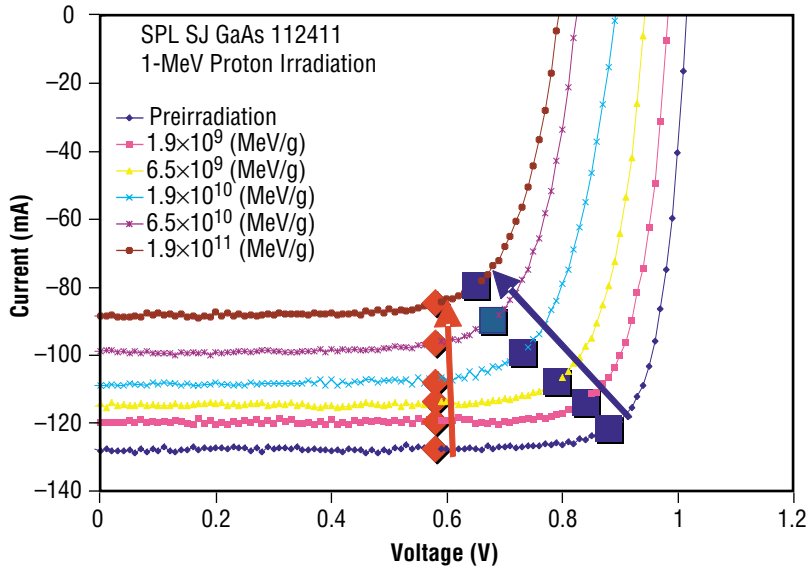
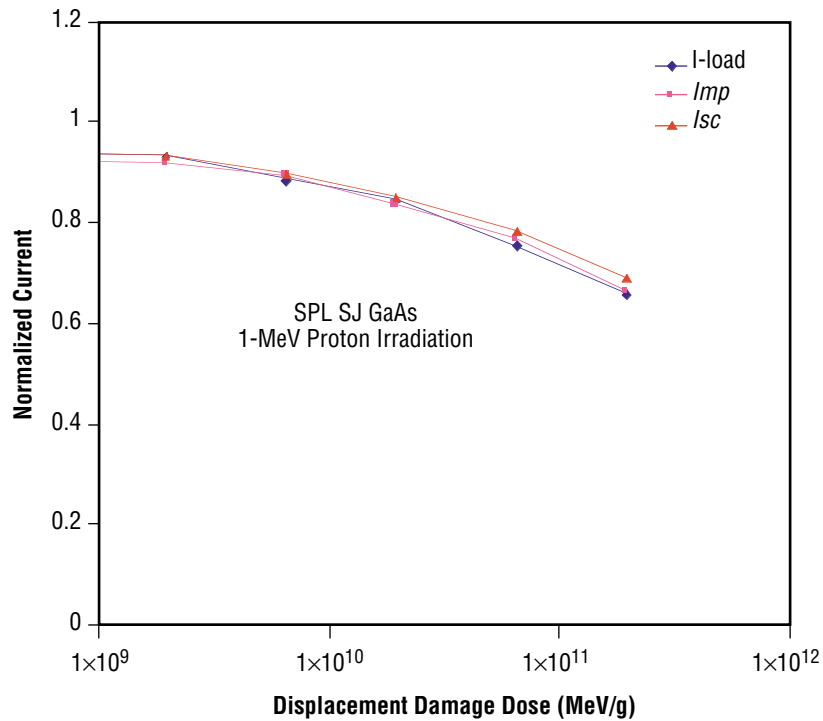Figure 6. IV curves measured on SJ GaAs solar cells that are representative of the cells on the MPTB array.

Figure 7. Current data taken from figure 6 that show that the three parameters demonstrate similar degradation characteristics, but that *Imp* is a better description of I-load than *Isc*.

4. SOLAR ARRAY VERIFICATION AND ANALYSIS TOOL CALCULATIONS

This section describes the process by which the SAVANT code produces a prediction of the solar array output as a function of time in orbit. This procedure begins with a determination and specification of the spacecraft orbit. Once the orbit has been defined, the SAVANT code implements a model to account for geomagnetic shielding and then calls on the NASA AP8 and AE8 computer codes to calculate the proton and electron radiation environments, respectively. With the radiation environment calculated, an analysis of the shielding effects of materials in contact with the solar cells is performed, which allows the spectrum incident directly upon the cell active region to be calculated. The program then reduces this spectrum to an equivalent value of *Dd* and uses the characteristic curve to calculate expected solar cell degradation level. This procedure is repeated for each day of the mission to create a degradation profile over mission lifetime that can be compared to the telemetered data shown in figure 2. Each of these procedural steps is described in sections 4.1–4.4.

4.1 Orbital Analysis

One of the major difficulties of this project was determining accurate orbital parameters for the host spacecraft because direct access to spacecraft operations personnel was not available. Therefore, calculations were performed in an iterative manner, being updated each time more accurate data were obtained. The first calculations were made with a crude approximation for the orbit of 39,200 × 1,200 km at 63° inclination for 1,000 days (2,000 orbits). However, Dyer et al. mention that there is a change in orbit perigee from 1,212 to 1,502 km between May 1998 and January 1999.[6] Considering the data in figure 2, the degradation rate does appear to lessen over time, which may be explained by an orbit change. Therefore, a second calculation was made for the orbit 39,185 × 1,185 km with 63.43° inclination, and then again for a hybrid orbit consisting of 39,158 × 1,212 km 63.43° inclination for 225 days, and then at 38,868 × 1,502 km with 63.43° inclination for 350 more days. Reference 6 does not comment on the apogee of the orbits, so the apogee was calculated assuming that the orbit maintains a 12-hr period, which fixes the semimajor axis.

At the end of this project, a detailed description of the actual ephemeris data was given (fig. 8). The SAVANT code was run with the hybrid orbit described above and with the detailed ephemeris data given in figure 8. As shown in the results, there is only a small difference between these two calculations in terms of the calculated solar cell degradation. This result supports the original choice of orbit. In addition, this highlights the speed and versatility of the SAVANT code as the code allows for rapid recalculation of the results for a given change in input parameters.

4.2 Radiation Environment Calculations

The calculation of the radiation environment within SAVANT is performed by an orbit generator, a geomagnetic shielding algorithm, and AP8 and AE8 models. This is accomplished by passing the ephemeris data to the orbit generator and particle environment calculation codes that are bundled as a part of SAVANT. This is a key point because performance predictions can only be as accurate as the
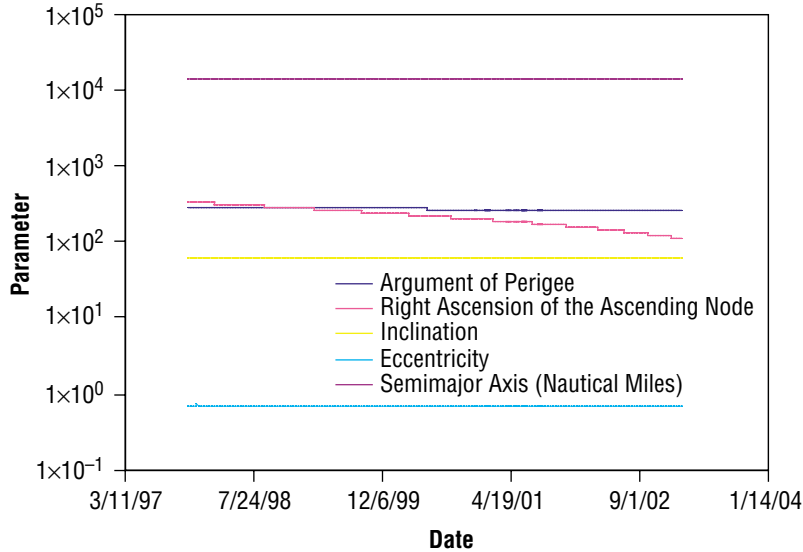
Figure 8. Ephemeris data for the MPTB spacecraft supplied
after the completion of the project.

environment calculations. As part of this project, time has been spent understanding exactly how AP8 and AE8 work and comparing their output with as much measured data as are available; the results of this analysis were presented by Dr. Morton.[7] This research provided insight into the accuracy of the environment calculations, which aided in the correlation of the measured and predicted solar cell data. Both the AP8 and AE8 programs advertise an inherent uncertainty factor of 2 due to scatter in the original data. AP8 and AE8 are static models that have not been updated since their releases in 1976 and 1991, respectively. They are based on satellite data taken between 1963 and 1970; 1970 was the lowest solar maximum of the space age. However, the radiation environment is not static. Therefore, the accuracy of the environment models is a factor of 2 at best.

4.3 Shielding Calculations

As an energetic particle traverses a material, it transfers some of its kinetic energy to the material so that the particle energy decreases and the particle slows down. It is this energy transfer that results in the radiation-induced damage in materials. Since the amount of damage produced is dependent on the particle energy, the change in energy experienced by a particle as it passes through materials before reaching the solar cell active region must be accounted for. This is done in SAVANT by the application of the continuous slowing-down approximation to the incident spectrum, whereby the slowed-down spectrum that emerges from the shielding material is calculated and is incident directly upon the solar cell active regions.[3,8]

Typically, solar cells are shielded on the front by a piece of glass and on the back by the solar array substrate. A schematic diagram of the MPTB solar array structure is shown in figure 9. The layers act to partially shield the solar cell from the incident particles. The SAVANT computer code that is under development in this project accounts for this shielding in predicting the radiation degradation of the solar array onorbit. The shielding properties of each of the layers and the coverglass are included in the SAVANT calculation of the slowed-down particle spectrum that is incident upon the solar cell. This is done by

11

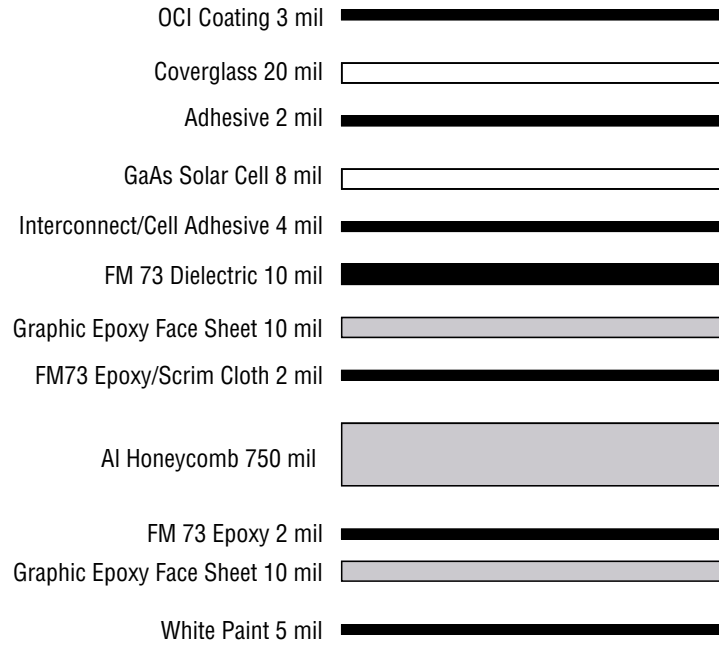| OCI Coating 3 mil |
| Coverglass 20 mil |
| Adhesive 2 mil |
| GaAs Solar Cell 8 mil |
| Interconnect/Cell Adhesive 4 mil |
| FM 73 Dielectric 10 mil |
| Graphic Epoxy Face Sheet 10 mil |
| FM73 Epoxy/Scrim Cloth 2 mil |
| Al Honeycomb 750 mil |
| FM 73 Epoxy 2 mil |
| Graphic Epoxy Face Sheet 10 mil |
| White Paint 5 mil |

Figure 9. Schematic diagram of the solar array structure
for the MPTB solar array.

reducing the multilayer stack to an equivalent thickness of solar cell coverglass using the densities of the materials. This is summarized in table 2 for the solar array itself; the values are reduced to an equivalent thickness of coverglass material at the bottom of the table. These data are used to determine the radiation shielding of the MPTB solar cells onorbit. It is seen that the rear-side shielding is equivalent to 31.25 mil of CMG coverglass. The slowed-down spectra calculated after the front shielding (cell coverglass) and the back shielding (solar array panel), are shown.

Table 2. Table of thickness and density of the layers
comprising the MPTB solar array.

Layer	Thickness (mil)	Density (g/cm^3)	Equivalent Thickness (mil g/cm^3)
Adhesive/interconnect	4	0.640	2.56
FM 73 dielectric	10	1.160	11.60
Graphite epoxy face sheet	10	1.650	16.50
FM 73 dielectric	2	1.160	2.32
Al honeycomb	750	0.032	24.00
FM 73 dielectric	2	1.160	2.32
Graphite epoxy face sheet	10	1.650	16.50
White paint	5	0.800	4.00
Total equivalent thickness	–	–	79.800
Density of coverglass (g/cm^3)	–	–	2.554
Total/CMG = equivalent coverglass (mil)	–	–	31.250

12

4.4 Equivalent Displacement Damage Dose Calculations

As is evident from figure 10, the resultant radiation environment impinging on the solar cells is complex, consisting of electrons and protons with energies extending continuously over a large range. Referring to section 3, the ground test data only allow for determining the solar cell degradation after irradiation by a monoenergetic particle. Thus, it is clear why a correlation method is required. With the NRL *Dd* method, the correlation is achieved by reducing the particle spectrum to an equivalent value of *Dd*. This is accomplished by integrating the slowed-down differential spectrum with the NIEL. As discussed briefly in section 3 and in detail in reference 5, the integration of the electron spectrum was performed assuming a dependence on NIEL to the power of 1.7.
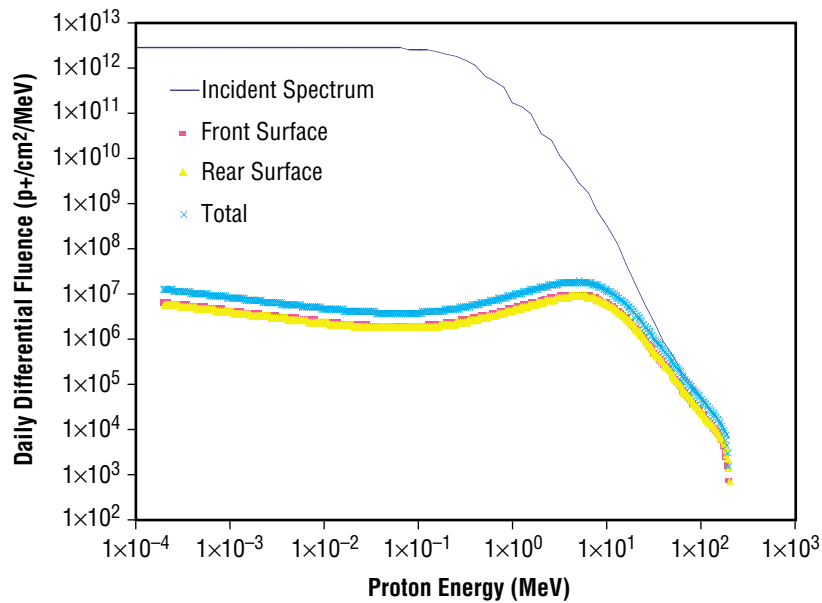
Figure 10. A graph of the proton spectra calculated by SAVANT for the MPTB orbit considering the first 1,600 days and assuming the ephemeris data from figure 8.

SAVANT implements these calculations iteratively over time at a user-defined time interval. For the MPTB mission, the accumulated *Dd* is calculated once a day; the results are shown in figure 11, assuming two of the orbits discussed in section 4.1. One of the orbits is the case where a single change in perigee occurring after 255 days in orbit was assumed. The other orbit was generated using the ephemeris data supplied to us late in the project. Until about April 2000, the two orbits result in essentially the same accumulated *Dd*. After that date, however, the orbit determined from the ephemeris data results in a lower accumulated *Dd*.

4.5 Solar Cell Performance Predictions

The necessary data are now available to predict the performance of the MPTB solar cells as a function of time in orbit. This is done by inserting the equivalent *Dd* values from figure 11 into the solar

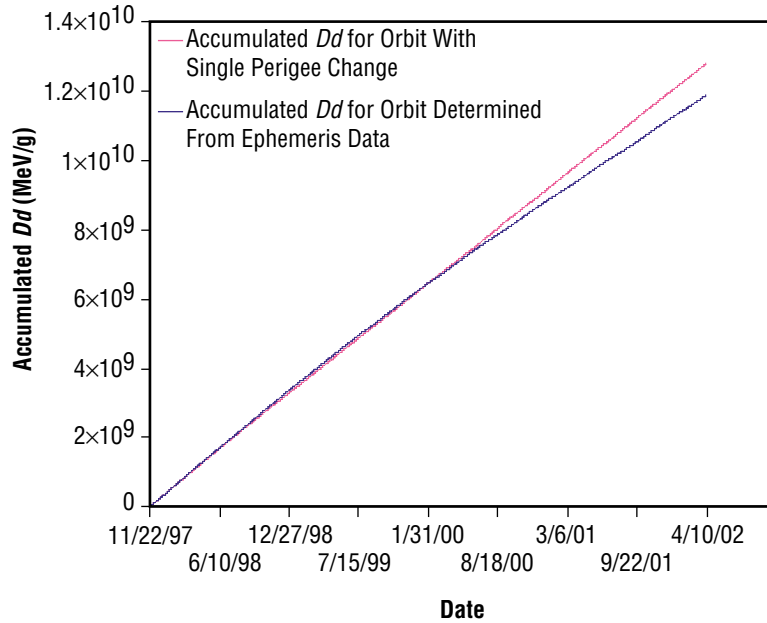Figure 11.   Equivalent *Dd* values accumulated by the MPTB
solar cells calculated for each day in orbit.

cell characteristic degradation curve (eq. (2)). The resultant data are shown in figure 12. The ephemeris data were used to generate the *Dd* values, and the degradation characteristics of *Imp* were used in the solar cell calculations. For discussion purposes, predictions assuming twice the amount of *Dd* appear to match the measured data more closely.

The predictions are seen to underestimate the measured solar cell degradation. In fact, the predictions appear to suggest that a factor of ≈2 in degradation exists between the calculated and measured data. This is shown by the red curve, which represents the calculated solar cell data if twice the estimated orbital *Dd* was used. In doing this, the calculated data are shifted to the left, thereby indicating more damage. Until August 2000, the data calculated assuming twice the *Dd* seem to agree with the measured data very well. After that date, however, there appears to be a reduction in the degradation rate in the measured data.

An indepth investigation to resolve this apparent discrepancy has been performed. This investigation made use of the onboard dosimeter data as discussed in section 5 and an analysis of the effect of solar event protons is discussed in section 6. Results of the investigation are presented in section 7.
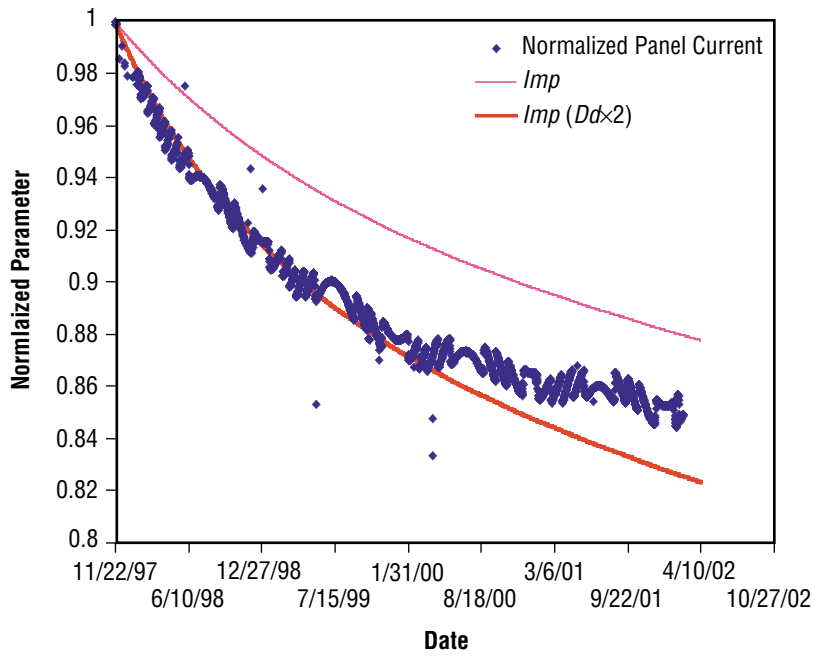
Figure 12.   Predicted solar array data from SAVANT compared to the measured data.

5. ONBOARD DOSIMETER ANALYSIS

The MPTB experiment has two different onboard particle detectors. One is the Cosmic Radiation Environment and Dosimetry (CREDO) experiment[6] that gives data of total fluence of protons per orbit with energy above 38 MeV. The other is the DSU, which gives similar data over four proton energy channels— 4, 6.5, 15, and 25 MeV. In this section, the data are analyzed and compared with the predictions from SAVANT.

The CREDO data, plotted in figure 13, are considered first. SAVANT was used to predict the total fluence of protons with energies >40 MeV received per orbit; these data are also shown in figure 13. Note that the data are shown as lines connecting the individual data points, and the lines appear to have a thickness. This is due to the fact that the even and odd orbits of MPTB alternatively pass through the South Atlantic Anomaly, so each orbit delivers different amounts of radiation to the spacecraft. Initially, SAVANT underpredicts the measured data by about a factor of 2. This is good agreement with the apparent factor of 2 underprediction of the solar array degradation seen in figure 12.
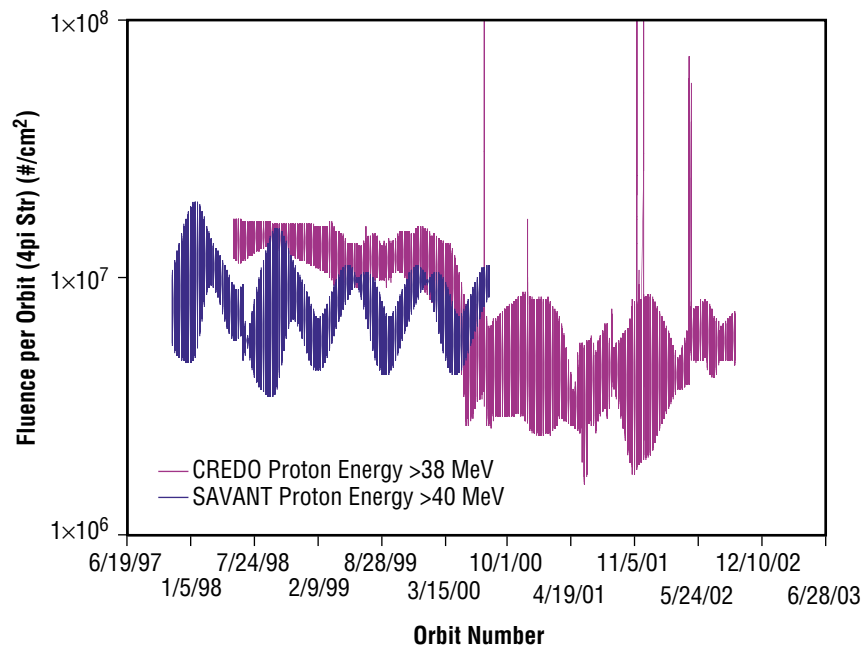

Figure 13. Values of total fluence of protons with energies <38 MeV absorbed each orbit by the CREDO experiment on MPTB along with similar data predicted by the SAVANT code.

It is very interesting to note that the CREDO data show a sharp drop in the total proton fluence absorbed after about 3/15/00 indicating a significant change in the radiation environment. This roughly coincides with the decrease in the degradation rate of the MPTB solar array output highlighted in figure 12. This change could be explained by a change in orbit, but the orbital data supplied do not show such a change (fig. 8).

The DSU data were then considered; however, only ≈1 yr of DSU data were received. The DSU data that measured the orbital fluence of protons with energies >25 MeV are plotted in figure 14 with the CREDO data from figure 13. Because of the lower energy cutoff for this DSU channel compared to the CREDO instrument, the DSU data were expected to be larger than the CREDO data. To the contrary, however, the DSU data are seen to be 2 to 3 times less than the CREDO data. Clarification on this result has been requested from the scientists responsible for the two instruments. There is significant speculation about the effect of the geometry of the two different instruments, but no adequate explanation has been forthcoming. Therefore, there is still a large uncertainty for the onboard radiation detectors.
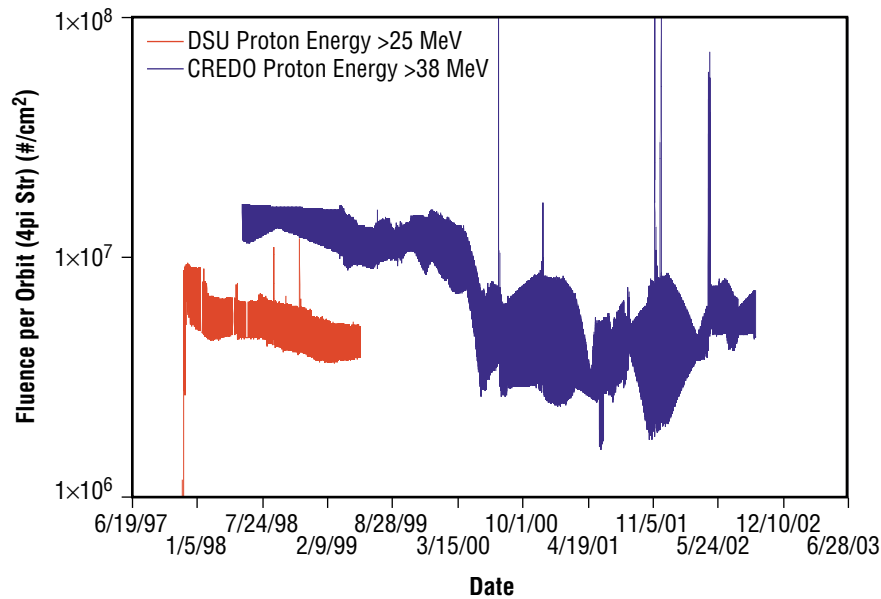
Figure 14.   Comparison of data measured by the two different onboard radiation detectors.

The DSU data are then compared with that predicted by SAVANT as shown in figure 15. In this figure, the DSU data are plotted for each of the four cutoff proton energies and shown as individual symbols. Again, the reason there appear to be two separate curves for each dataset is the effect of the odd and even MPTB orbits. A prediction made by SAVANT of the orbital fluence of protons with the cutoff energies of the DSU is plotted as well. These data are shown as solid lines connecting the data points.

One initial observation to be made concerns the low energy DSU data. Most of the >4-MeV DSU data either overlap or drop below the 6-MeV data. These results are not yet clearly understood.
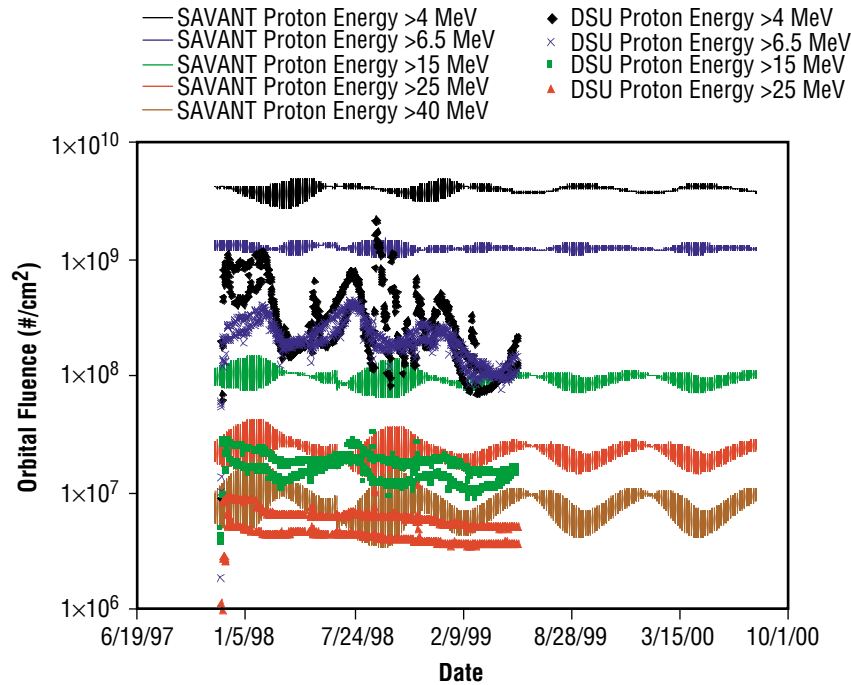
Figure 15.   DSU data for each of the four cutoff energies compared with data calculated by SAVANT. The SAVANT calculations are consistently greater than the DSU measured data.

For each of the datasets, SAVANT calculates more protons than measured by the DSU. This is in contrast to the case of the CREDO data where SAVANT calculated fewer protons by about a factor of 2. This leaves the question of which onboard dosimeter is correct. Considering that the factor of 2 suggested by the CREDO data results in the SAVANT calculations aligning very well with the measured data. Considering also that the CREDO data correlate well with the measured solar array data in terms of the decrease in degradation rate after about March 2000 lends credence to the CREDO data. However, firm conclusions cannot be made. One conclusion that can be drawn is that there is significant uncertainty in the measured and calculated radiation environments; therefore, the fact that the solar array predictions match the measured data within a factor of 2 can be considered a reasonably good result.

18

6. SOLAR EVENT ANALYSIS

The CREDO data, shown again in figure 16, have also been used to quantify the amount of proton fluence incident on the MPTB spacecraft due to solar events. Also shown in figure 16 are the CREDO data where the proton fluence, detected while the spacecraft was within the trapped proton belts, have been subtracted out. The spikes in the remaining data correspond to solar proton events. Considering the data in this fashion shows that while the solar events do produce large fluxes of protons for a short time, the vast majority of the protons incident on the spacecraft come from the trapped proton belts. The additional protons produced by solar proton events are relatively small in number.

The data in figure 16 suggest that the effect of the solar event protons will be minimal on the MPTB solar arrays. An analysis to quantify this result was performed. A SAVANT calculation with a solar proton spectrum using the 7/14/00 flare was run and the equivalent proton Dd was 1.9×10^6 MeV/g. This is about the same as ten days in the MPTB orbit. Given that the mission spans thousands of days, 10 days is not significant and will not noticeably change the slope of the solar cell damage curves. In figure 16, the magenta curve represents that total CREDO data that has already been shown. The blue curve represents the amount of proton fluence measured by the CREDO instrument when the spacecraft was outside of the trapped proton belts. The spikes in the remaining data correspond to solar proton events.
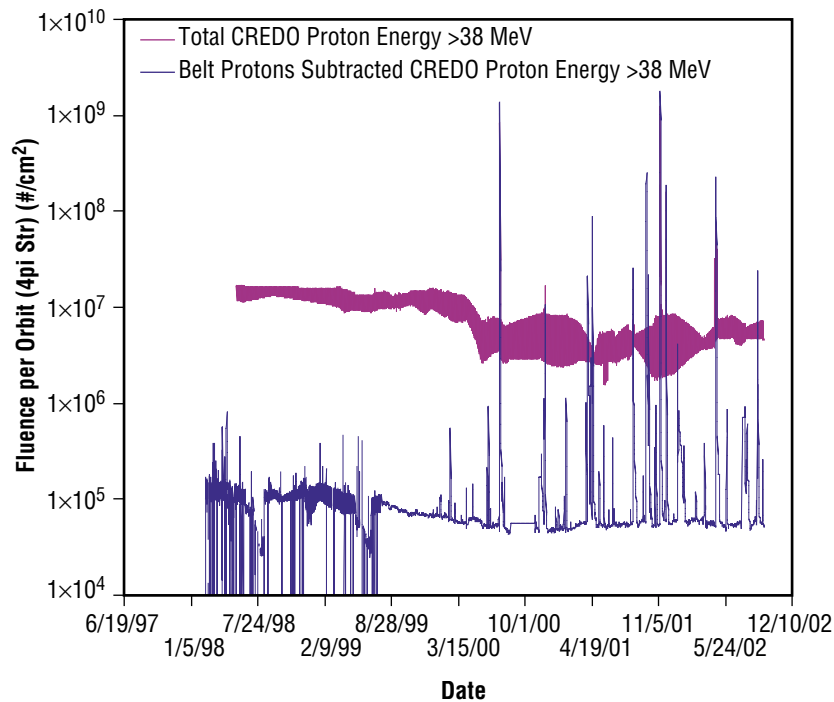

Figure 16.   Plot of the CREDO data.

7. DISCUSSION OF SOLAR ARRAY VERIFICATION AND ANALYSIS TOOL RESULTS

The data in figure 12 represent the best effort at predicting the on-orbit solar array data; the predictions are accurate to within a factor of 2. While this result is within the stated uncertainties of the environment models,[7] better agreement is achieved between the SAVANT predictions and measured on-orbit data for other missions.[8,9] One difference with MPTB is that this is, by far, the longest ever considered. Over 4 yr of MPTB data are available from this mission compared to <2 yr for the next longest mission. This means that the predictions are especially sensitive to temporal variations in the radiation environment since such variations are not accounted for in the AP8 model. In addition, the solar cells on MPTB have a 20-mil thick coverglass, which is more than three times the thickness of the thickest coverglass analyzed in the past. This means that a portion of the proton spectrum is being considered at much higher energies than in past studies.

Another point to note is that this is the highest apogee mission that has been studied. Therefore, AP8 is being used in a region not previously investigated. Also, in this orbit, the spacecraft experiences higher electron fluences than have been analyzed in the past. All of the previous missions were almost exclusively proton environments, so the model has yet to be fully validated in such a mixed environment. NRL is currently funded in FY 2003 to study device response in a mixed electron and proton environment.

The primary area of uncertainty in the present calculations lies in the environment predictions. Considering only the higher energy proton of the incident proton spectrum, the CREDO data suggest that AP8 underestimates the environment by a factor of 2. Increasing the predicted Dd values by this amount brings the predicted solar array output into very close agreement with the measured data at least up to March 2000. Beyond this date, there appears to have been a change in the radiation environment of the spacecraft. There are no details of this, so it has not been accounted for. This factor of 2 discrepancy between the measured data and AP8 calculations is in agreement with the Combined Release and Radiation Effects Satellite (CRRES) dosimeter measurements that indicate that AP8 underpredicts the flux for energies >10 MeV and overpredicts the flux for lower energies.[10] Since only protons with incident energies greater than ≈8 MeV can pass through the 20-mil coverglass on the MPTB solar cells, the MPTB solar cell degradation is expected to track the higher energy portion of the spectrum. Therefore, it may be concluded that the calculated results presented here are in good agreement with the measured values where the primary cause of uncertainty lies in the environment models.

To be complete, the DSU data should be discussed at this point. SAVANT predictions of the radiation environment are consistently higher than the DSU data. For the 4- and 6.5-MeV DSU channels, the predictions are in agreement with the present discussion since CRRES demonstrated AP8 to overpredict the fluence of protons at lower energies except that the difference is much larger than expected. For the 15- and 25-MeV channels, however, the opposite result would have been expected. Also, the 4- and 6.5-MeV channel data are not consistent with each other, and 25-MeV channel DSU data do not agree with the CREDO data. With these as yet unexplained inconsistencies, it is difficult to draw any meaning from the DSU data so that those data serve only to add to the overall uncertainty in the environment description.

8. GRAPHICAL USER INTERFACE FOR SOLAR ARRAY VERIFICATION AND ANALYSIS TOOL

Dr. Morton has created a version of SAVANT that runs on Microsoft Windows® with a graphical user interface (GUI). This provides a user-friendly interface for specifying the orbit and solar cell before calculating the damage for the mission. Figure 17 shows the input screen. The input is roughly divided into mission (including orbit and solar conditions) and solar cell. As the user enters either the apogee or semimajor axis, the program automatically disables the alternate parameter. As the second parameter is input, the program calculates the alternate entries, and fills them in. If the user wishes to enter additional orbit data; e.g., argument of perigee or right ascension, the "Other Orbital Options" button can be selected.

Currently, the "Launch Date" option, which would account for variation of Earth-Sun distance and automatically determine solar maximum or minimum conditions, and the "Back of Cell" option, which accounts for the back surface shielding, are not functional. To account for the back surface irradiation, one must perform a separate run and the *Dd* value to that obtained considering the front surface; i.e., coverglass.

Once the mission and solar cell have been entered, the user presses the "Calculate Damage" button. When the calculation is finished, the results are displayed in the right-hand window, as total accumulated *Dd*, and the scaled maximum power $P_{\max}/P_0$.

There is limited capability to add new solar cell types and materials to the program in anticipation of new solar cell architectures. However, the materials that are currently in the program have been tested and verified in some fashion, with some compared to flight experiments and others compared to ground experiments. Adding new materials may require some consultation with the software authors.
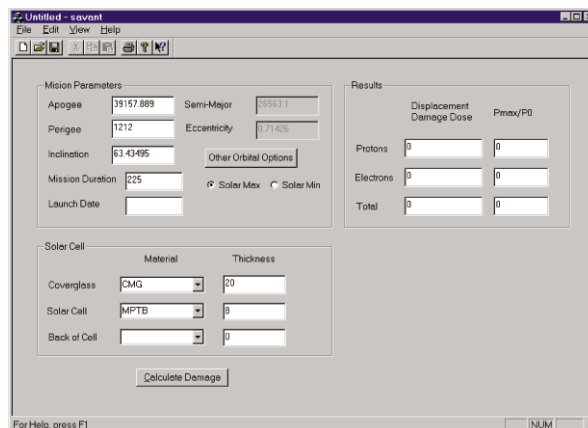

Figure 17.   Input screen for the SAVANT GUI.

21

9. QUANTIFYING LOW ENERGY PROTON EFFECTS

Dr. Messenger, in close collaboration with Mr. Ed Burke who is working under Dr. Mike Xapsos's Space Environments and Effects project, has made huge breakthroughs in this area. He adapted the methodology to accurately account for damage produced by low energy protons. Furthermore, he has adapted the methodology to account for the case of protons incident upon devices with thick active regions, such as silicon (Si) solar cells.

The issue is that the lower the incident energy of the proton, the more rapidly it will lose energy to displacement in the lattice. If the incident energy is low enough, the proton will slow down and stop within the material. This is illustrated in figure 18 for the case of a proton incident upon a multijunction indium gallium phosphide (InGaP)/GaAs/Ge solar cell. The data in figure 18 were calculated using the stopping and range of ions in matter (SRIM).[11] The device depicted here is representative of the current state of the art for high efficiency space solar cells. Protons with incident energies <400 keV are seen to stop within the active region of the device. Since the NIEL increases rapidly with decreasing energy by ≈1/E dependence, this results in a large amount of *Dd* being deposited into the device active region. Furthermore, if the proton energy is changing as it passes through the device active region, then the NIEL associated with that proton is also changing. Thus, a calculation of the equivalent *Dd* using the NIEL based on the incident energy will result in a significant underestimation. While this does not have a major impact on the analysis of thin devices like the multijunction cell depicted in figure 18, it represents a significant limitation of our methodology in analyzing thick devices, such as Si solar cells. Indeed, until now, Si solar cells could not be included in the SAVANT database.
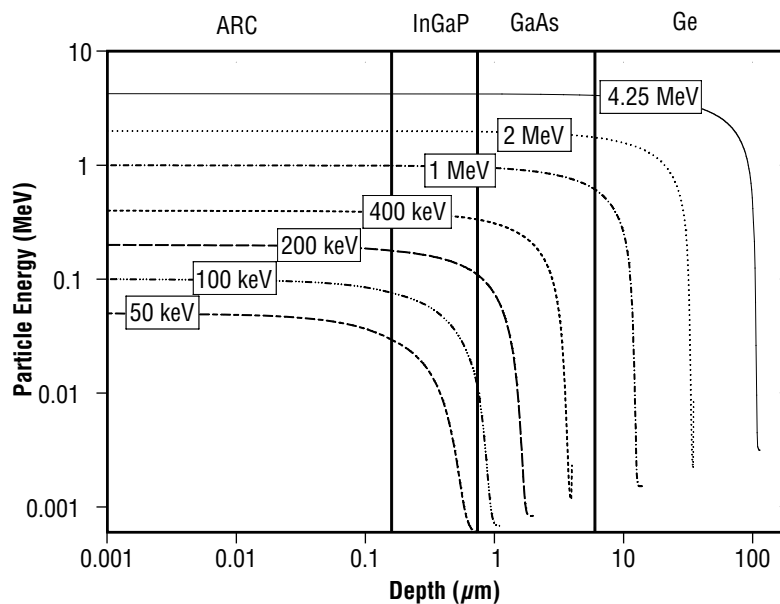

Figure 18. Calculation of the energy of a proton incident upon a multijunction InGaP/GaAs/Ge solar cell as a function of depth into the solar cell for protons having several incident energies.

The breakthrough came with Mr. Burke devising a method for calculating an effective NIEL for the case when the proton energy is changing as it passes through the device active region. The method consists of using SRIM to calculate the number of vacancies that are produced by the irradiation as a function of depth into the material, from which the NIEL is then calculated using the Kinchin-Pease Model[12] (fig. 19). The integral of these NIEL values over the active region of the device is then used to generate an effective NIEL value for that incident proton energy. For solar cells, the active region is typically defined as equivalent to two diffusion lengths from the junction. It is by using this effective NIEL value that the proper value of Dd for the specific irradiation may be attainted.
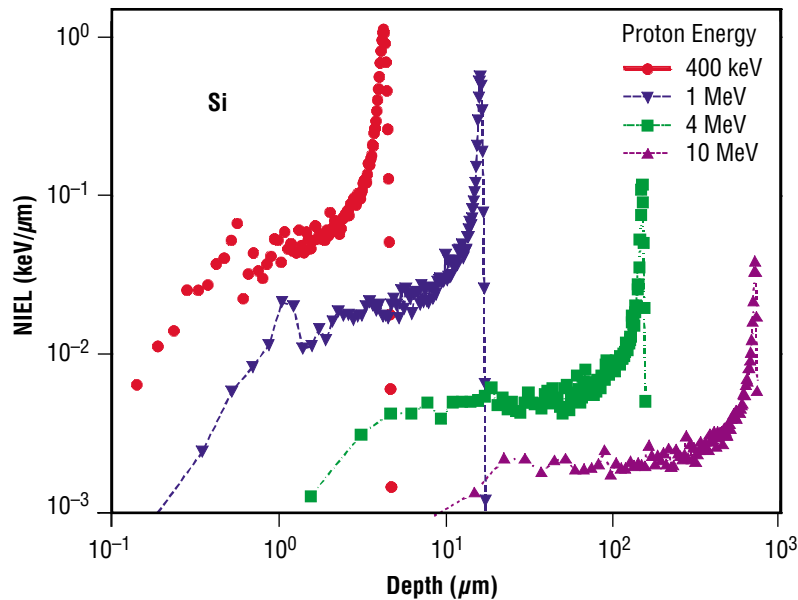

Figure 19.   NIEL values calculated as a function of depth
into a-Si solar cells determined using SRIM.

Dr. Messenger developed a calculation methodology that implements this series of calculations for protons of various energies incident upon devices of various materials and active region widths or, alternatively, diffusion lengths. An example of the results for the most important case of Si solar cells is shown in figure 20. Also shown in figure 20 are the relative damage coefficients (RDCs) measured in the Si solar cells.[4] The RDCs indicate the amount of damage induced in the solar cell by a proton of a specific energy relative to that produced by a proton at a reference energy, typically chosen to be 10 MeV. The basis of the Dd methodology is that the energy dependence of the RDCs is given by the NIEL. However, the Si NIEL, when calculated using the incident proton energy, does not track the solar cell RDCs for energies less than $\approx$6 MeV. The effective NIEL, on the other hand, is seen to model the measured RDCs quite well over the entire energy range. Two sets of effective NIEL values are shown corresponding to two assumptions of diffusion length, which defines the active region width. Therefore, solar cell performance predictions based on Dd values calculated using the effective NIEL will be expected to be accurate.
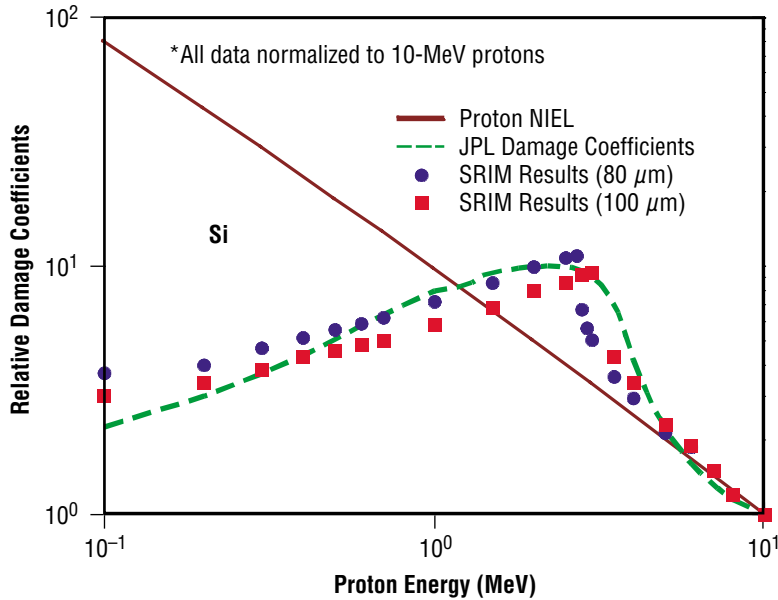
Figure 20.   A comparison of the NIEL values determined using the new method developed in this program with the measured relative damage coefficients for the Si solar cells.

Dr. Messenger is also in the process of applying this improved methodology to the case of multijunction solar cells as depicted in figure 18. Given that these devices are quite thin in comparison to the proton ranges, a large effect is not expected. Indeed, the effects may turn out to be negligible when considering the case of a true space spectrum. However, the solar cell community has made a large issue of the effect of low energy protons on these multijunction devices, so it is instructive to perform this analysis. Also, the RDCs for the multijunction display interesting behavior in the low energy regime. This behavior is demonstrated in figure 21 where the RDCs for several technologies from two separate solar cell vendors, SPL and Tecstar, are shown[13] and compared to the GaAs NIEL, normalized to 10 MeV. The 2J label refers to a two-junction InGaP/GaAs device while the 3J label refers to a three-junction InGaP/GaAs/Ge device. Efforts are currently underway to accurately model the inflection point observed near 100 keV. A proton with incident energy of 100 keV comes to rest in the transition region between the InGaP and GaAs layers (fig. 18). For all of the devices, this results in less relative damage, and for some, the Tecstar 3J in particular, there is a significant dip in the data. The goal is to accurately model these results using knowledge of the internal cell structure and a careful implementation of SRIM. The first attempt at this is shown in figure 22, and indeed, the double-hump behavior appears in the modeled data.

The long-term implications of these results are worth highlighting. With the improved calculation methodology developed in this project, the radiation damage induced by protons of essentially any incident energy incident upon a variety of device materials and structures can be modeled with only a knowledge of the material parameters and internal device dimensions. Thus, when complete, SAVANT will be capable of predicting the on-orbit response of an arbitrary cell structure. This will enable trade studies to be performed on new cell and proposed cell designs with little or no measured data.

Dr. Messenger presented these results at the NSREC conference[14] and as an invited talk at the Fifth International Workshop on Radiation Effects on Semiconductor Devices for Space Application in Tuksuba, Japan.[15]
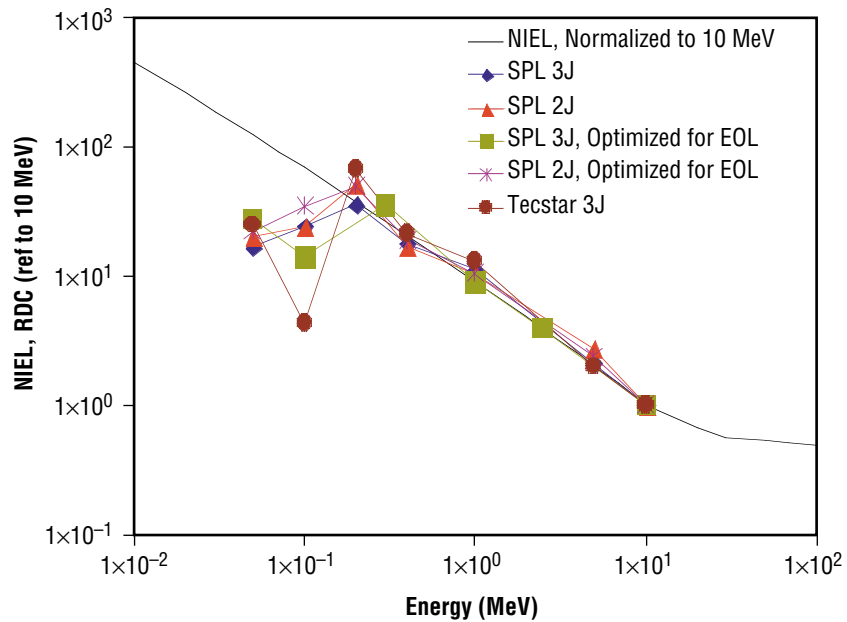

Figure 21. Comparison of the RDCs from several multijunction solar cell technologies from two solar cell vendors and the GaAs NIEL normalized to 10 MeV.
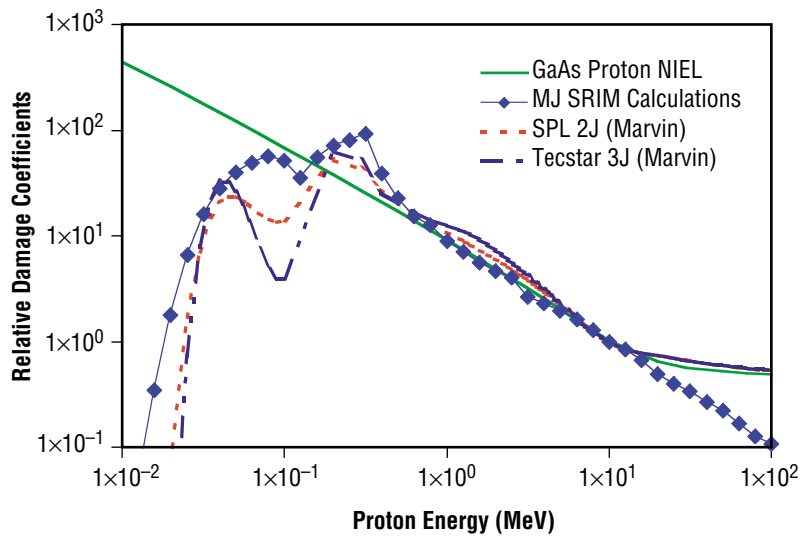

Figure 22. Data representing our initial attempt to model the "double hump" observed in the multijunction solar cell RDC curve.

10. EXTENDING THE MODEL TO MULTIJUNCTION SOLAR CELLS

The data shown in figure 21 have another valuable interpretation. For the majority of the energy range studied, the RDCs vary linearly with the GaAs NIEL. This means that the Dd methodology can be directly applied to these devices. The procedure is to fit the data from the various technologies to equation (2) as was done for the MPTB single-junction GaAs cells. This has been done and, as an example, the results for the SPL 3J cells under proton irradiation are shown in figure 23. The fitting parameters for the Pmp data of the multijunction cells under proton and electron irradiation are given in table 3. Using these parameters and results, SAVANT is now adapted to include multijunction solar cells.
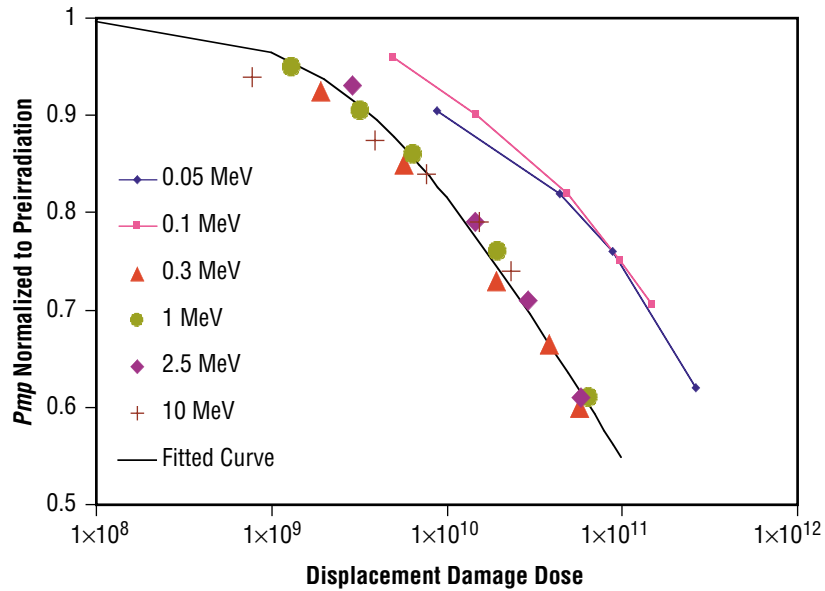

Figure 23.   *Pmp* degradation data for the SPL 3J EOL cells from reference 14 plotted as a function of *Dd* with the solid curve representing a fit of the data to equation (2).

Table 3.   Fitting parameters determined from fitting the multi-junction *Pmp* data from reference 14 to equation (2).

	Protons		Electrons		
	C	Dx (MeV/g)	C	Dx (MeV/g)	n
SPL 3J	0.27	1.70×10^9	0.31	5.143×10^9	1.4
SPL 3J EOL	0.30	3.17×10^9	0.26	7.492×10^9	1.7
SPL 2J	0.30	2.56×10^9	0.31	6.07×10^9	1.1
SPL 2J EOL	0.30	3.28×10^9	0.28	7.281×10^9	1.0
Tecstar 3J	0.25	1.04×10^9	0.27	3.437×10^9	1.2

11. EXTENDING THE MODEL TO THIN FILM SOLAR CELLS

Thin film solar cells (TFSCs) are a rapidly emerging technology for space applications. The two primary technologies under development are amorphous Si (a-Si) and copper indium (gallium) disellenide (CuIn(Ga)Se$_2$) (CIGS). Considering the a-Si cells, electron and proton irradiation data on these cells have been generated. The response of the *Pmp* parameter to the irradiations are shown in figure 24. Note that the data are plotted as a function of particle fluence. In the case of proton irradiation, very little variation is seen among the three energies. In the electron irradiation case, the lower energy irradiation is seen to cause the most degradation. These results are not consistent with the *Dd* methodology, so it is not expected that these cells can be readily included in the SAVANT code. It appears that, in these amorphous materials, the amount of solar cell damage cannot be directly related to the amount of displacement damage calculated assuming a crystalline Si lattice.
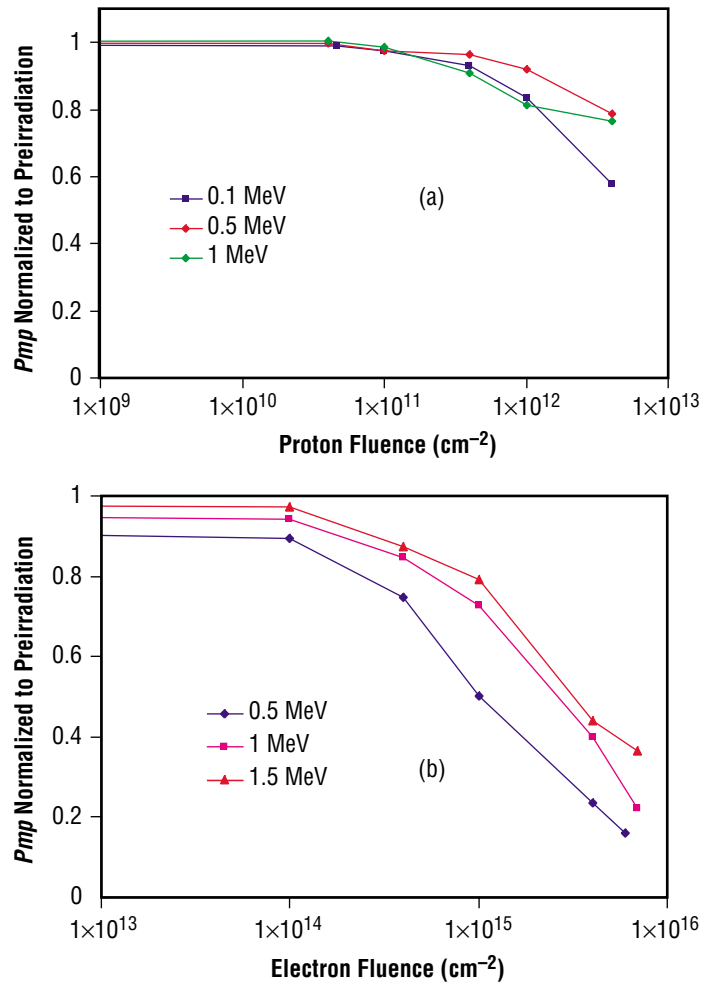

Figure 24. Data depicting the response of *Pmp* in a-Si solar cells to (a) proton and (b) electron irradiation.

It is worth noting here that these a-Si solar cells undergo significant annealing of radiation damage at temperatures as low as 60 °C. To demonstrate this, one set of a-Si solar cells was subjected to a 24-hr, 60 °C thermal anneal after each irradiation fluence. The data do not follow the trends predicted by the *Dd* methodology. The results measured after the 1-MeV electron irradiations are shown in figure 25. When the annealing is included, these cells display extreme radiation resistance.

Data on CIGS solar cells have also been collected. A summary of the available CIGS data is shown in figure 26. The CIGS cells on metal and on glass were measured while the other data were drawn from the literature.[16–20] There is some scatter in these data, such as a variety of cell structures and overall device quality, since the data span many years. Nevertheless, the data do appear to fit the *Dd* methodology. The solid and dashed curves represent a fit of the proton and electron data to figure 26, respectively. The electron data employed a value of 2 for the *n* parameter indicating a quadratic dependence on NIEL. The fit parameters are given in table 4. These data have been transferred to the SAVANT code so that SAVANT is now capable of addressing thin film, CIGS devices.

It should also be noted here that the CIGS cells do display a relatively low annealing temperature, like the a-Si cells. Significant research is currently underway to measure and quantify this CIGS annealing. The next step in development will be to incorporate this annealing into the on-orbit end-of-life (EOL) performance predictions.
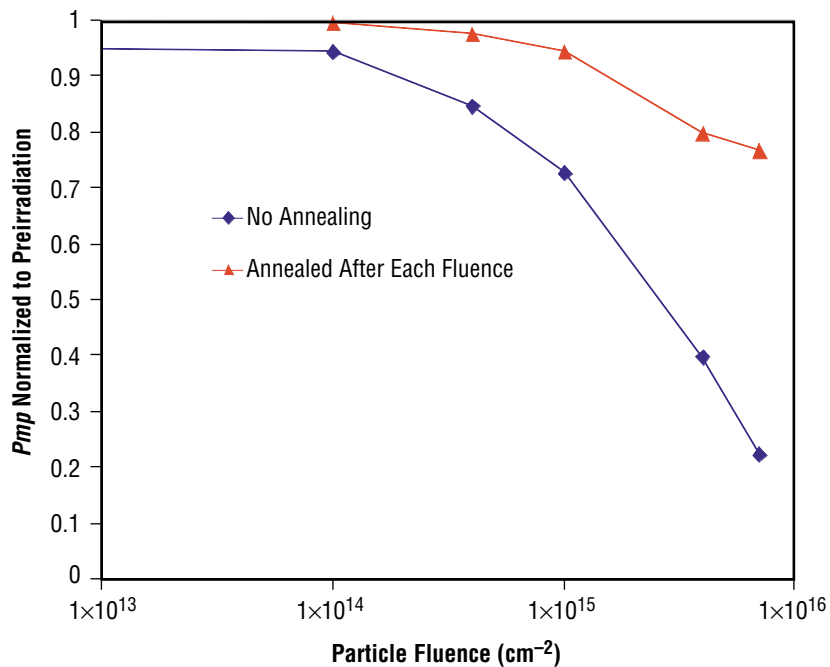

Figure 25.   1-MeV electron irradiation data for the a-Si solar cells where data that included a 24-hr, 60 °C thermal anneal after each irradiation fluence are compared to data taken without an annealing step.
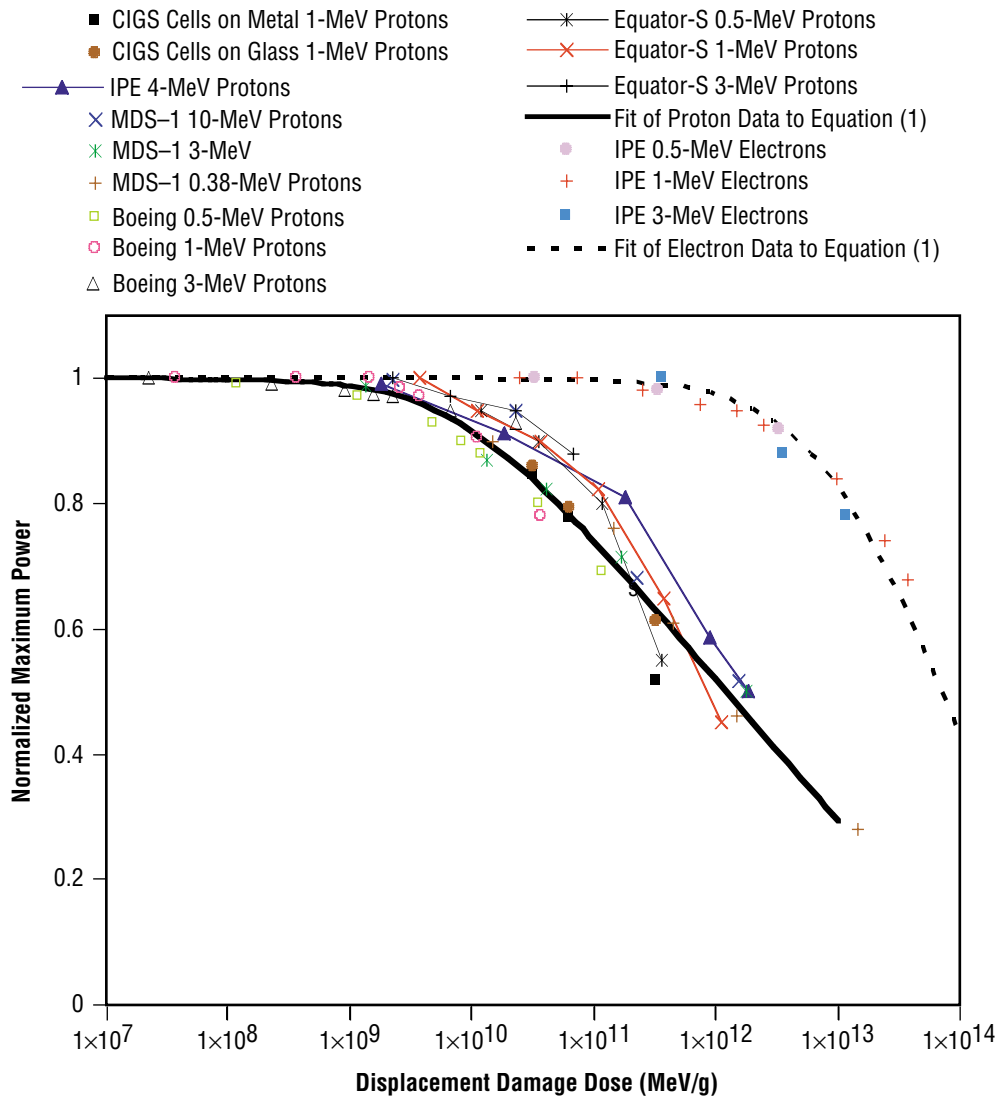
Figure 26.   Proton and electron irradiation damage measured in CIGS solar cells.

Table 4. Fitting parameters determined for the CIGS TFSCs.

Proton Data					
	C	dC	Dxp	$dDxp$	
Pmp	0.226	0.012	7.54×10^9	5×10^7	
Electron Data					
	C	dC	Dxe	$dDxe$	Rep	n
Pmp	0.508	0.146	8.28×10^{12}	7.31×10^{12}	44.52	2

REFERENCES

1. Brown, M.R.; Garcia, C.A.; Goodelle, G.S.; Powe, J.S.; and Schwartz, J.A.: "Characterization Testing of Measat GaAs/Ge Solar Cell Assemblies," *Prog. In Photovoltaics: Res. and App.*, Vol. 20, p. 129, 1996.

2. Marion, J.B.: *Classical Dynamics*, Sections 8.8–8.9, pp. 258–265, Academic Press, New York, 1986.

3. Summers, G.P.; Messenger, S.R.; Burke, E.A.; Xapsos, M.A.; and Walters, R.J.: "Low Energy Proton-Induced Displacement Damage in Shielded GaAs Solar Cells in Space," *Appl. Phys. Lett.*, Vol. 71, p. 832, 1997.

4. Anspaugh, B.E.: *GaAs Solar Cell Radiation Handbook*, Jet Propulsion Laboratory Publication 96–9, 150 pp., July 1, 1996.

5. Summers, G.P.; Burke, E.A.; Shapiro, P.; Messenger, S.R.; and Walters, R.J.: "Damage Correlations in Semiconductors Exposed to Gamma, Electron, and Proton Radiations," *IEEE Trans. Nucl. Sci.*, Vol. 40, pp. 1372–1379, December 1993.

6. Dyer, C.S.; Truscott, P.R.; Sanderson, C.; Watson, C.; Peerless, C.L.; Knight, P.; Mugford, R.; Cousins, T.; and Noulty, R.: "Radiation Environment Measurements From CREAM and CREDO During the Approach to Solar Maximum," *IEEE Trans. Nucl. Sci.*, Vol. 47, p. 2208, December 2000.

7. Morton, T.L.: "Estimation of the Radiation Environment Based on the NASA AP–8 and AE–8 Models," in *Proceedings of the Fifth International Workshop on Radiation Effects on Semiconductor Devices for Space Applications*, Takasaki, Japan, p. 7, October 9–11, 2002.

8. Messenger, S.R.; Walters, R.J.; Summers, G.P.; Morton, T.; La Roche, G.; Signorini, C.; Anzawa, O.; and Matsuda, S.: "A Displacement Damage Dose Analysis of the COMETS and Equator-S Space Solar Cell Flight Experiments," in *Proceedings of the 16th European Photovoltaic Solar Energy Conference and Exhibition*, pp. 243–247, Glasgow, Scotland, May 1–5, 2000.

9. Morton, T.L.; Chock, R.; Long, K.; Bailey, S.; Messenger, S.R.; Walters, R.J.; and Summers, G.P.: "Use of Displacement Damage Dose as an Engineering Model of GaAs Solar Cell Radiation Damage," *Technical Digest of the 11th International Photovoltaic Science and Engineering Conference*, pp. 815–816, Sapporo Hokkaido, Japan, September 1999.

10. Gussenhoven, M.S.; Mullen, E.G.; Brautigam, D.H.; Holeman, E.; Jordan, C.; Hanser, F.; and Dichter, B.: "Preliminary Comparison of Dose Measurements on CRRES to NASA Model Predictions," *IEEE Trans. Nuc. Sci.*, Vol. 38, Issue 6, pp. 1,655–1,662, December 1991.

11. Ziegler, J.F.; Biersack, J.P.; and Littmark, U.: *The Stopping and Range of Ions in Solids*, Vol. 1, Pergammon Press, New York, 1985. (SRIM is freely available at http://www.srim.org.)

12. Kinchin, G.H.; and Pease, R.S.: *J. Nucl. Energy*, Vol. 1, p. 200, 1955.

13. Marvin, D.C.: "Assessment of Multijunction Solar Cell Performance in Radiation Environments," Aerospace Report No. TOR–00(1210)–1, 2000.

14. Messenger, S.R.; Burke, E.A.; Summers, G.P.; and Walters, R.J.: "Application of Displacement Damage Dose Analysis to Low-Energy Protons on Silicon," *IEEE Trans. Nuc. Sci.*, Vol. 49(6), pp. 2,690–2,674 December 2002.

15. Messenger, S.R.; Burke, E.A.; Summers, G.P.; and Walters, R.J.: "Modelling Low Energy Proton Effects on Solar Cells," in *Proceedings of the Fifth International Workshop on Radiation Effects on Semiconductor Devices for Space Applications*, Takasaki, Japan, p. 95, October 9–11, 2002.

16. Jasenek, A.; and Rau, U.: "Defect Generation in CuIn(Ga)Se$_2$ Heterojunction Solar Cells by High-Energy Electron and Proton Irradiation," *J. Appl. Phys.*, Vol. 90, p. 650, 2001.

17. Contreras, M.A.; Tuttle, J.; Gabor, A.; Tennant, A.; Ramanathan, S.; Asher, S.; Franz, A.; Keane, J.; Wang, L.; Scofield, J.; and Noufi, R.: "High Efficiency Cu(In,Ga)Se$_2$-based Solar Cells: Processing of Novel Absorber Structures," in *Proceedings of the 24th IEEE Photovoltaic Specialists Conference*, Piscataway, NJ, p. 68, December 1994.

18. Hartmann, M.; Schmidt, M.; Jasenek, A.; Schock, H.W.; Kessler, F.; Herz, K.; and Powalla, M.: "Flexible and Light Weight Substrates for Cu(In,Ga)Se$_2$ Solar Cells and Models," in *Proceedings of the 28th Photovoltaic Specialists Conference*, Anchorage, AK, p. 638, 2000.

19. Tuttle, J.R.; Szalaj, A.; and Keane, J.: "A 15.2% AMO/1433 W/kg Thin-Film Cu(In,Ga)Se$_2$ Solar Cell for Space Applications," in *Proceedings of the 28th IEEE Photovoltaic Specialists Conference*, Anchorage, AK, p. 1,042, 2000.

20. Mueller R.L.; and Anspaugh, B.E.: "Results of Some Initial Space Qualification Testing of Triple Junction a-Si and CuInSe$_2$ Thin-Film Solar Cells," in *Proceedings of the 12th Space Photovoltaic Research and Technology Conference*, Cleveland, OH, p. 108, October 20–22, 1992.

REPORT DOCUMENTATION PAGE

Form Approved
OMB No. 0704-0188

1. AGENCY USE ONLY *(Leave Blank)*	2. REPORT DATE August 2004	3. REPORT TYPE AND DATES COVERED Technical Publication

4. TITLE AND SUBTITLE

Displacement Damage Effects in Solar Cells—Mining Damage From the Microelectronics and Photonics Test Bed Space Experiment

5. FUNDING NUMBERS

6. AUTHORS

R.J. Walters, T.L. Morton,* and S.R. Messenger**

7. PERFORMING ORGANIZATION NAMES(S) AND ADDRESS(ES)

Naval Research Laboratory
4555 Overlook Avenue, S.W.
Washington, DC 20375

8. PERFORMING ORGANIZATION REPORT NUMBER

M–1119

9. SPONSORING/MONITORING AGENCY NAME(S) AND ADDRESS(ES)

NASA's Space Environments and Effects (SEE) Program
George C. Marshall Space Flight Center
Marshall Space Flight Center, AL 35812

10. SPONSORING/MONITORING AGENCY REPO NUMBER

NASA/TP—2004–213338

11. SUPPLEMENTARY NOTES

Prepared for NASA's Space Environments and Effects (SEE) Program by The Naval Research Laboratory
Technical Monitor: Donna Hardage, NASA Marshall Space Flight Center
*Ohio Aerospace Institute, Cleveland, OH   **SFA, Inc., Largo, MD

12a. DISTRIBUTION/AVAILABILITY STATEMENT

Unclassified-Unlimited
Subject Category 93
Available: NASA CASI 301–621–0134

12b. DISTRIBUTION CODE

13. ABSTRACT *(Maximum 200 words)*

The objective is to develop an improved space solar cell radiation response analysis capability and to produce a computer modeling tool which implements the analysis. This was accomplished through analysis of solar cell flight data taken on the Microelectronics and Photonics Test Bed experiment. This effort specifically addresses issues related to rapid technological change in the area of solar cells for space applications in order to enhance system performance, decrease risk, and reduce cost for future missions.

14. SUBJECT TERMS

radiation, solar cells, solar array, current, fluence, irradiation, proton, electron, ground test, displacement damage

15. NUMBER OF PAGES

44

16. PRICE CODE

17. SECURITY CLASSIFICATION OF REPORT Unclassified	18. SECURITY CLASSIFICATION OF THIS PAGE Unclassified	19. SECURITY CLASSIFICATION OF ABSTRACT Unclassified	20. LIMITATION OF ABSTRACT Unlimited